Eur Biophys J (1993) 22:309–321

European Biophysics Journal


# The viscoelasticity of entangled actin networks: the influence of defects and modulation by talin and vinculin

**R. Ruddies, W. H. Goldmann, G. Isenberg, E. Sackmann**

Department of Physics (Biophysics group), Technical University of Munich, James-Franck-Strasse, D-85748 Garching, Germany

Received: 18 March 1993 / Accepted in revised form: 5 July 1993

**Abstract.** Rheological measurements of the frequency-dependent complex elastic module $G^*(\omega)$ of entangled F-actin solutions in the frequency range $10^{-5} - 1$ Hz were carried out in three dynamic regimes: *1.)* A terminal relaxation from gel-like to liquid-like behaviour measured at frequencies $\omega \leq \tau_d^{-1}$, *2.)* a rubber-type plateau and *3.)* a regime determined by chain conformational transitions at frequencies $\omega > \tau_i^{-1}$. A major point of interest was to clarify whether rheological, high precision measurements can yield quantitative information about the influence of talin and vinculin on the structure, chain dynamics, elasticity and viscoelasticity of actin filaments with time. We show that in the regime reflecting internal chain dynamics ($10^{-2}$ to 1 s time domain), F-actin behaves as a random coil of the Rouse type. This contrasts with dynamic light scattering and correlation spectroscopic studies of actin filament flickering, which indicate that filaments behave as semiflexible rods. The internal chain dynamics, which are determined by thermically excited bending undulations, exhibit a persistence length of 0.3–1 μm. Evidence is provided that this discrepancy is due to a cross-over of semiflexible rod behaviour at excitation wavelengths ($\Lambda$) below approximately 1 μm to random-coil behaviour at $\Lambda \gg 1$ μm (expected at a frequency $\omega \sim 1$ Hz). The random coil behaviour is largely determined by defects in actin filaments leading to sharp bends of the chain which act as semiflexible hinges. Talin produces drastic effects on the time course of viscoelasticity during actin polymerization. It promotes the rapid formation of short filament fragments ($\sim 1$ μm, within time scales of min) which anneal slowly into long filaments (within several hours), most probably by fusion. The viscoelasticity depends on the coexistence of short and very long filaments indicated by the elongation of the rubber plateau. The most dramatic effect is a reduction of the ratio of the terminal ($\tau_d$) to the Rouse relaxation time of $\tau_i$ by more than one order of magnitude ($\tau_d/\tau_i = 100$ compared to ratio $\tau_d/\tau_i = 2000$ for pure actin). From this it is concluded that talin causes a remarkable decrease in the effective segment length of the macromolecule and, thus induces an increase in chain stiffness. Vinculin on the other hand shows no such effect.

**Key words:** Rheology – Semiflexible biopolymers – Cytoskeletal viscoelasticity – Actin-talin-vinculin interaction – Binding defects

*Correspondence to:* E. Sackmann

## Introduction

Actin network formation is of great interest because of its vital role for cell architecture. Further, actin networks gained importance as models of macromolecular solutions and gels of semiflexible and polyelectrolytic filaments (Korn et al. 1987; Sato et al. 1987; Schmidt et al. 1989; Janmey et al. 1990; Müller et al. 1991).

Networks with mesh sizes of the order of micrometers allow the application of optical techniques (Schmidt et al. 1989) in order to study the fundamental sructural and dynamic properties by applying scaling laws of entangled macromolecular solutions and gels (Schmidt et al. 1989; Müller et al. 1991; Kaufmann et al. 1991; Piekenbrock and Sackmann 1992). In addition, a variety of actin binding proteins are available by which the structure of the networks (e.g. length of the filaments, degree of entanglement or degree of cross-linking) may be manipulated in a controllable and reversible manner (Wegner 1982; Pollard and Cooper 1986). By applying quasielastic light scattering (QELS) studies of the internal dynamics of actin filaments, we found a broken power law for the relation between the decay constant, $\Gamma(Q,t)$ of the conformational excitations of the chain and the excitation wavevector $Q = 2\pi/\Lambda$ of the form $\Gamma(Q,t) \propto t\,Q^{2.75}$ (Piekenbrock and Sackmann 1992). Recently, it was shown by Farge and Maggs (1993) that this power law is expected if the internal chain dynamics are determined by bending undulations. For so-called Rouse chains composed of chains of beads interconnected by entropy springs, a remarkably different power law $\Gamma(Q,t) \propto t\,Q^3$ was expected, provided

a strong hydrodynamic interaction exists between the beads. Further, it was shown by direct correlation spectroscopic analysis of the chain excitations visualized by fluorescence microscopy that the mean square amplitudes scale with the reverse of the fourth power of the undulation wavevector $Q$: $\langle U_Q^2 \rangle \propto k_B T/BQ^4$ ($B$, being the bending elasticity modulus) as expected for bending undulations. A persistence length of the order of $L_p \sim 1$ μm was obtained. However, it was also found that the bending model holds only for wavelengths $\leq 1$ μm, whereas at longer wavelengths the chains appear much stiffer.

The bending model contrasts with results of our previous rheological studies of dilute and semidilute F-actin solutions (Müller et al. 1991). We found that in the frequency regime where the viscoelasticity is determined by the internal chain dynamics, the actin filaments behave like Rouse chains. Support for this conclusion was given by the finding that actin solutions exhibit scaling laws typical for synthetic macromolecular solutions.

In this paper we present evidence that the discrepancy between the rheological and optical studies can be explained in terms of a high density of chain defects within the actin filaments, which anneal very slowly ($\sim 20$ h). The elastic response and mechanical relaxation probed by rheological measurements at low frequency ($10^{-5}$–1 Hz) are determined by the dynamics of the defects whilst these are dominated by the overdamped bending undulations in the frequency regime ($\sim 10^3$ Hz) probed by QELS.

We further show that once the physical basis of the viscoelastic processes are known, rheological measurements may be used to evaluate suitable effects of actin binding proteins (here: talin and vinculin) on the structure and dynamics of actin networks in a quantitative way. Continuous measurements at fixed frequencies allow the study of elasticity behaviour of developing actin networks with high sensitivity in the presence and absence of these two proteins.

Talin promotes the rapid nucleation and formation of short ($\sim 1$ μm) actin filaments (Kaufmann et al. 1991, 1992; Goldmann et al. 1992) which slowly anneal into long filaments. It is shown that the frequency dependence of the storage and loss modulus of pure F-actin and F-actin-talin solutions can be reproduced by superimposition of reptation and Rouse type relaxation processes. The effective segment length of the Rouse-like chain is decreased by a factor of approximately 4–5 when actin is polymerized in the presence of talin. Talin has also a remarkable stiffening effect on actin filaments.

Vinculin, however, when complexed with actin exhibits similar features to pure actin (Goldmann et al. 1992).

## Materials and methods

*Reagents*

2 mM Tris-HCl, pH 7.5; 0.2 mM $CaCl_2$, 0.2 mM ATP, 0.5 mM DTT (= G-buffer); actin was polymerized in: 10 mM imidazole, 1 mM EGTA, 1 mM ATP and 2 mM $MgCl_2$; pH 7.5 (= F-buffer).

*Proteins*

Actin was prepared according to Spudich and Watt (1971) from acetone powder obtained from rabbit back muscle, followed by a gel filtration step as described by MacLean-Fletcher and Pollard (1980). Fractionated G-actin beyond the elution peak (at $\sim 1$ mg/ml) was stored in G-buffer at 4 °C.

Platelet talin and vinculin were isolated from outdated human thrombozytes by the Collier and Wang (1982) method. Talin was further purified by passing it through a gel filtration column (Kaufmann et al. 1991). After the first ionic exchange column according to this protocol, vinculin was purified by an additional hydroxylapatite column and eluted by a linear gradient from 0.02 M to 0.4 M $KH_2PO_4$.

Proteins were purified to homogeneity as judged by SDS mini slab gels (cf. Goldmann et al. 1992). Protein concentrations were determined according to Bradford (1976).

*Rotation disk rheometer*

The apparatus has been described in detail by Müller et al. (1991). Basically, it consists of a cylindrical glass cuvette with an inner radius of $r_i = 7$ mm and a volume of $\sim 1.5$ ml. The base of the cuvette is mounted in an aluminium thermostated holder, which is in thermal contact with the solution. Temperature control is achieved by Peltier elements situated in the holder. A glass disc of $r = 6$ mm is placed on the surface of the viscoelastic solution. On top of the disc a magnet with dimensions of $1 \times 1.2$ mm$^2$ and a $2 \times 2$ mm$^2$ deflection mirror are mounted; the plane of the latter forming an angle of 45° with the horizontal line. The glass cuvette is surrounded by two perpendicularly oriented magnetic coils. One of these serves to fix the orientation of the disc and the other (the deflection coils) to apply an oscillatory shear force to the viscoelastic liquid. The voltage of the deflection coils is computer controlled. The "in-phase" and "out-of-phase" component of the rotational amplitude, $\alpha(t)$ of the disc are analysed as follows: The beam of a He–Ne-laser incident in a vertical direction along the rotational axis of the disc is horizontally deflected by the mirror mounted on the disc. Its horizontal orientation is recorded by a gradient photodiode. The amplified response of the diode is evaluated by computer.

The actin solution in the measuring cuvette is covered by a phospholipid monolayer (dimyristoylphosphatidylcholine) which is essential to avoid the gelation of actin owing to its denaturing at the air/water interface (Müller et al. 1991). Moreover, it ensures good mechanical contact to the glass disc which is covered by a monolayer of octadecyltrichlorosilane.

*Data evaluation*

The theoretical basis of the rheometer and the details of the data analysis have been discussed previously (Müller

et al. 1991). As a reminder and in order to introduce the definitions required in the following the basic principles of the rotating disc rheometer are briefly summarized:

The viscoelasticity of the actin solution is determined by the complex shear modulus

$$G^*(\omega) = G'(\omega) + i\,G''(\omega) \tag{1}$$

where, $G'(\omega)$ is the frequency-dependent storage modulus and $G''(\omega)$ the loss modulus. The latter is related to the dynamic viscosity of the fluid according to $\eta'(\omega) = G''(\omega)/\omega$. For high viscosities and low shear rates ($d\alpha/dt$), the shear field within the viscoelastic layer decays exponentially. If the radius (R) of the cylindrical layer is large compared to its height (h) boundary effects at the circumference of the glass cylinder can be neglected. The maximum frequency of measurement $\omega$: $D_\omega \exp(i\,\omega\,t)$ which is exerted by the driving coils, storage and loss moduli are obtained from the following equations:

$$\frac{D_\omega}{\alpha_\omega}\cos\varphi = -\omega^2\,\Theta + M_x + C\,G'(\omega) \tag{2}$$

$$\frac{D_\omega}{\alpha_\omega}\sin\varphi = C\,G''(\omega) \tag{3}$$

where $\alpha_\omega$, is the amplitude of the orientational deflection and $\varphi$, is the phase shift between the excitation and the response. $M_x$ is the torque exerted by the magnetic coils determining the resting orientation; $\Theta$ is the moment of inertia of the disc, and $C$ is a geometry factor given by $C = \pi R^4/2\,\mathrm{h}$ (cf. also Ferry 1980). The above equations yield relative values of the viscoelastic constants. In order to obtain absolute values, the torque $M_x$ must be measured. This has only been determined by calibration with different glycerol-water mixtures (Müller et al. 1991). (Note: Owing to the Kramers-Kronig-relation the influence of the instrument starts at the same frequency for both the real and imaginary value of $G'$ and $G''$).

The sensitivity of the rheometer is approximately 1 mPa, corresponding to the lower limit of the actin concentration of $\sim 10$ µg/ml. The maximum measuring frequency is about 5 Hz since at higher frequencies the viscoelastic response is dominated by the instrument. Most measurements were performed down to $10^{-5}$ Hz.

## Results

### *Pure entangled F-actin solutions*

*Three dynamic regimes.* Figure 1 shows the measurements of the storage modulus $G'(\omega)$ and the loss modulus $G''(\omega)$ of polymerized actin (= F-actin) at $c_A = 300$ µg/ml ($\sim 7$ µM). The measurement was performed over five frequency decades (log scale), and three regimes of well defined power laws are clearly observed:

*1)* The terminal transition to the fluid (= sol) state is characterized by a drop of $G'(\omega)$ and the maximum of $G''(\omega)$ yield (cf. Fig. 8; "Simulation" below), which is observed much more clearly than in our previous work (Müller et al. 1991). Although the decay to zero of $G''(\omega)$ at $\omega \to 0$ can not be observed directly, the terminal relaxation time, $\tau_d$ is obtained from the frequency at which the value of $G'(\omega)$ has dropped to half of the value in the plateau regime: $\tau_d \sim 4 \cdot 10^{-5}$ s.

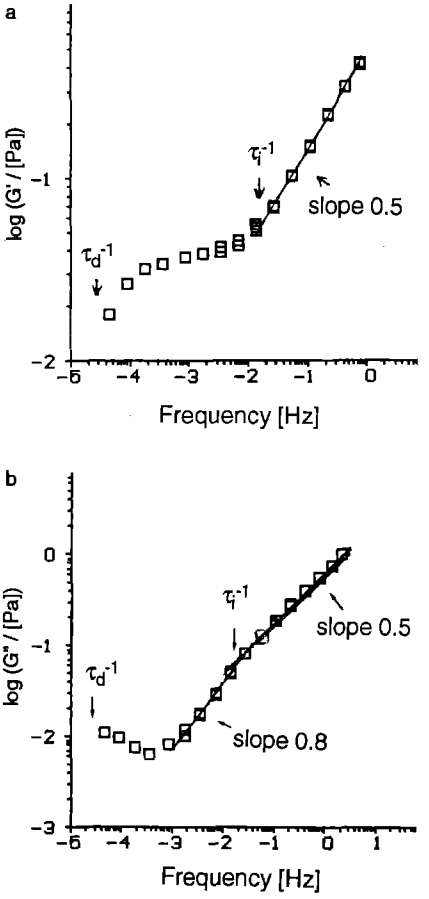


**Fig. 1.** Frequency dependence (log scale) of **a** the storage modulus $G'(\omega)$ and **b** the loss modulus $G''(\omega)$ of an F-actin solution at monomer concentration $c_A = 300$ µg/ml (approximately 7 µM). The data points at $\omega \geq 1$ Hz are modified by contributions of the instrument. The sample was polymerized at 20°C for 4 h, heated to 36°C for two hours and cooled down again to 20°C. The measurements, which were started after annealing at 20°C for approximately 6 h, lasted for approximately 2 h

*2)* The plateau regime of $G'(\omega)$ extending from $10^{-4} \leq \omega \leq 10^{-2}$ Hz is clearly developed although $G'(\omega)$ exhibits a finite slope. It can be observed that the regime $G''(\omega)$ exhibits an ascending branch where $G''(\omega)$ scales with $\omega$ as $G''(\omega) \propto \omega^{0.8}$.

*3)* At $\omega \geq \tau_i^{-1}$, $G'(\omega)$ exhibits an ascending branch characterized by a $G'$-vs.-$\omega$ power law of the form $G'(\omega) \propto \omega^{0.5}$; simultaneously, the slope of the $\log G''(\omega)$-vs.-$\log \omega$ curve also changes from 0.8 to $0.54 \pm 0.02$. In this regime the dynamic elasticity is determined by the internal dynamics of the actin filaments. $\tau_i$ is the longest relaxation time of the slowest mode of the whole spectrum of internal relaxation processes. The value of $\tau_i$ is a first approximation obtained from the frequency (a) of the onset of the ascending branch of $G'(\omega)$ and (b) of the change in slope of $G''(\omega)$ with $\tau_i \approx 10^2$ s. The finding of a well-defined power law $G'(\omega)$, $G''(\omega) \propto \omega^z$ over two frequency decades is essential for the interpretation of the

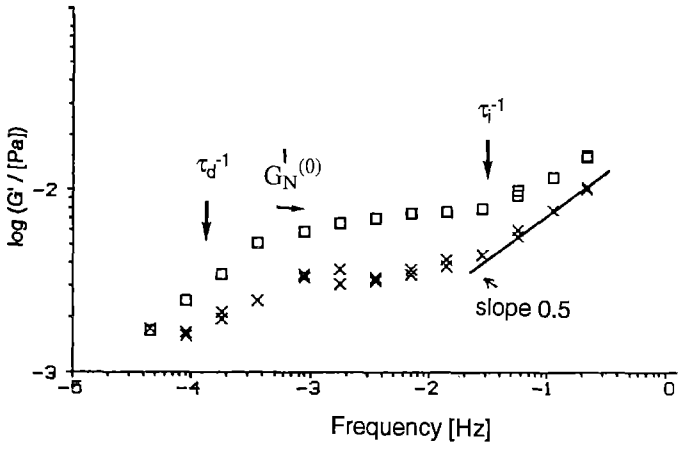


**Fig. 2.** Evaluation of "long time" annealing of an F-actin solution at a concentration of $c_A = 100$ μg/ml measured at 25°C. Data points (×) show the measurement of the storage modulus $G'(\omega)$ which was started 2 h after polymerization. Data points (□) show a second measurement, which was started after the completion of the first run. It corresponds to about 20 h after the start of polymerization. *Note:* $G_N^{(0)}$ = rubber plateau

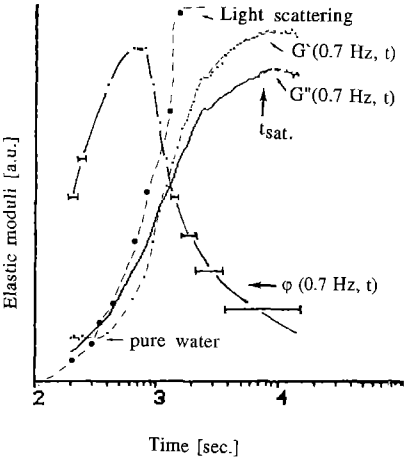


**Fig. 4.** Evolution of viscoelasticity during the nucleation and growth of actin filaments. The storage modulus (– · –) and the loss modulus (——) were measured at $\omega = 0.7$ Hz. The phase shift, $\varphi$ (0.7 Hz, $t$) (...) was calculated from the measured values of $G'$ (0.7 Hz, $t$) and $G''$ (0.7 Hz, $t$). The points are measured data and the lines are drawn to guide the eye. The actin concentration was $c_A = 300$ μg/ml (~7 μM) and the measuring temperature was 20°C. Measurements by static light scattering are also shown (Piekenbrock 1991). *Note:* [a.u.] = arbitrary units

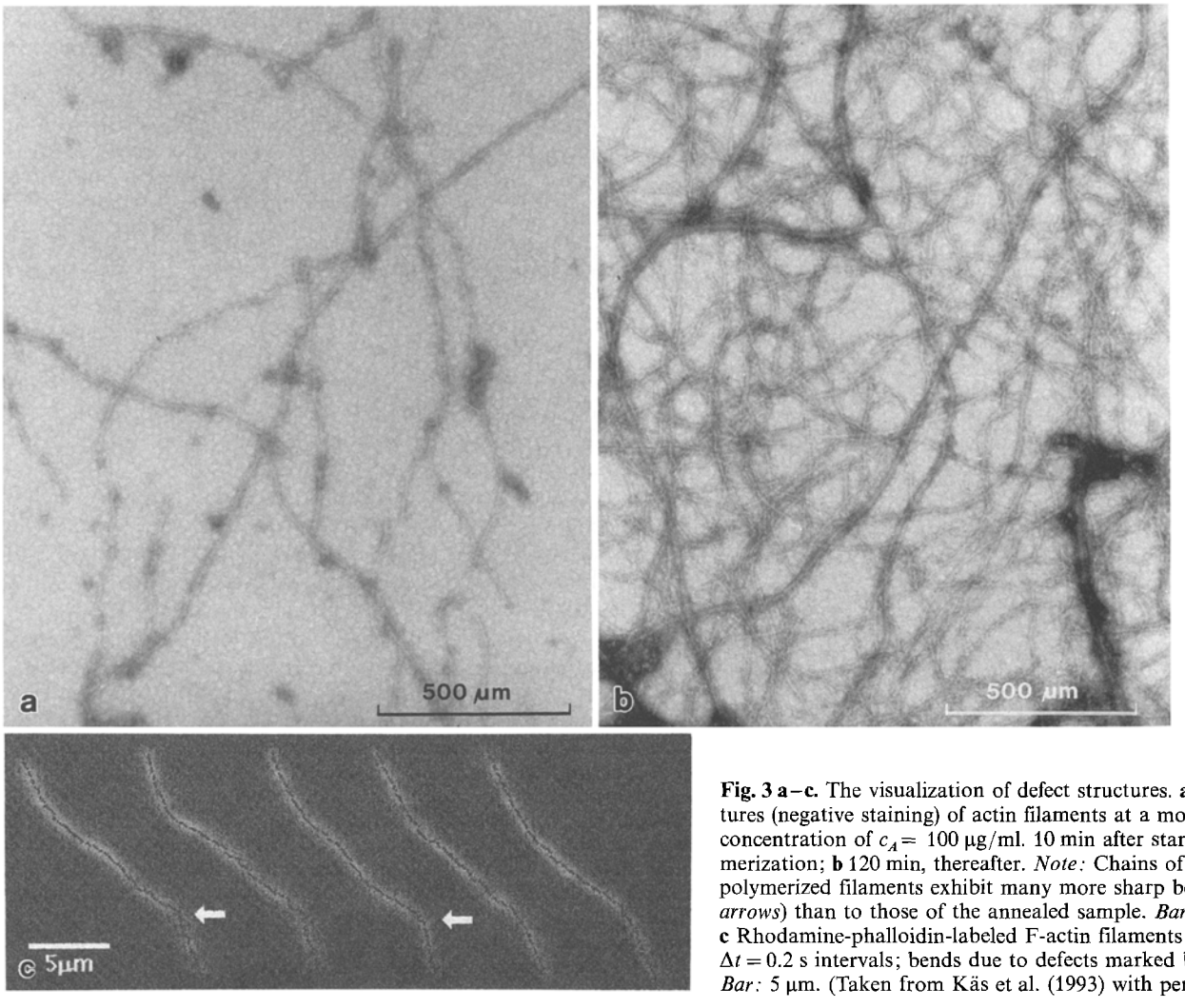


**Fig. 3 a–c.** The visualization of defect structures. **a** EM pictures (negative staining) of actin filaments at a monomer concentration of $c_A = 100$ μg/ml. 10 min after start of polymerization; **b** 120 min, thereafter. *Note:* Chains of freshly polymerized filaments exhibit many more sharp bends (cf. *arrows*) than to those of the annealed sample. *Bar:* 500 nm. **c** Rhodamine-phalloidin-labeled F-actin filaments at $\Delta t = 0.2$ s intervals; bends due to defects marked by arrow. *Bar:* 5 μm. (Taken from Käs et al. (1993) with permission)

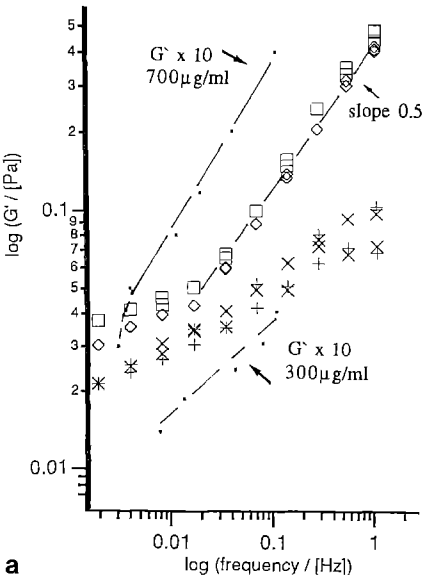


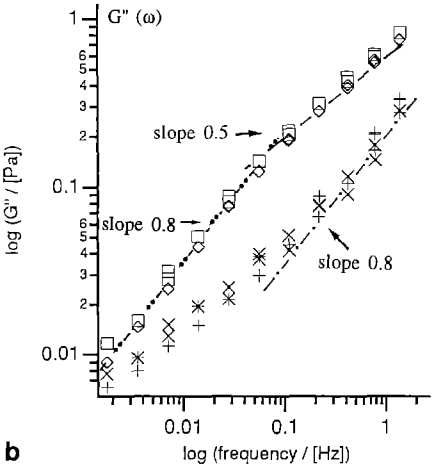


**Fig. 5 a, b.** Effect of talin and vinculin on the frequency dependence of viscoelastic parameters. The actin concentration was 300 µg/ml and the measuring temperature 25 °C. **a** Storage modulus for pure F-actin (□); for F-actin and vinculin at molar ratio $r_{AV} = 3$ (◇); for F-actin and talin at molar ratio $r_{AT} = 7$ (×); for F-actin in presence of vinculin and talin at $r_{AT} = r_{AV} = 10$ (+). For comparison we also show the $10 \times G'(\omega)$ curves for solution of F-actin in the presence of *severin* (data points: the 10 fold value of the measured $G'(\omega)$ are plotted in order to limit the ordinate). **b** Loss modulus for 300 µg/ml pure F-actin (□), for F-actin in presence of vinculin at molar ratio $r_{AV} = 3$ (◇); for F-actin and talin at $r_{AT} = 7$ (×); and for F-actin with talin and vinculin at $r_{AV} = r_{AT} = 10$ (+)

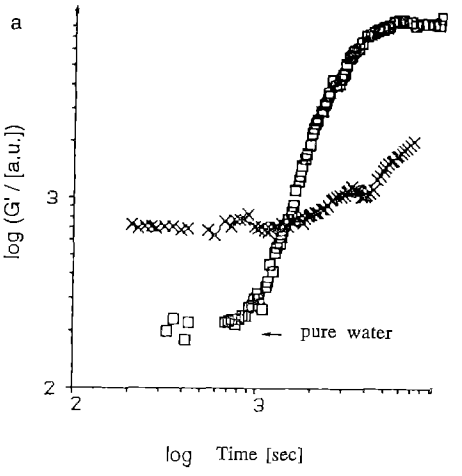


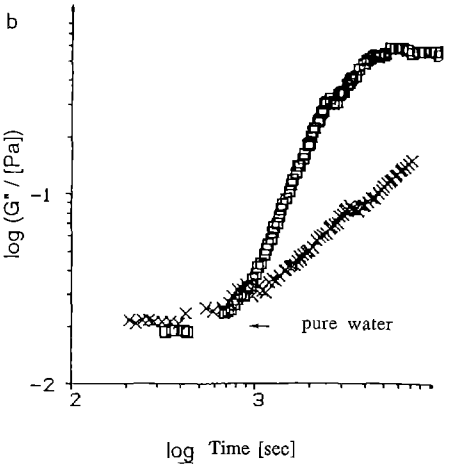


**Fig. 6 a, b.** Comparison of time evolutions of viscoelasticity of F-actin solution (of concentration $c_A = 300$ µg/ml) in the absence (*data points* □) and the presence of talin at an actin:talin molar ratio of $r_{AT} = 7$ (*data points* ×) at 20 °C

mechanical relaxation processes in terms of a molecular model.

### *Annealing of transient actin networks*

Previously, it was reported by Piekenbrock and Sackmann (1992) that freshly polymerized F-actin exhibits a considerable number of sharp bends which where attributed to packing faults (= defects) within one strand of the double helix and that these defects appear after a few hours. To test this hypothesis the viscoelastic moduli versus frequency curves where taken repeatedly. Figure 2 shows the result for a solution of $c_A = 100$ µg/ml. The first measurement was started approximately 4 h after polymerization and lasted for approximately 12 h; the second measurement ($\log G'(\omega)$ – vs – $\log \omega$) was performed thereafter. Since the measurements are always started at the low frequency end, the plateau regime of the first run corresponds to the situation of about 6 h of annealing. Figure 2 shows that the plateau regime of freshly polymerized actin is much less pronounced than after 24 h of annealing. The terminal relaxation regime of the fresh F-actin solution stretches out, although the terminal relaxation time $\tau_d$ (defined as the reciprocal frequency for which $G'(\omega)$ is half the plateau value of $G_N^0$) does not change appreciably. As shown below, the elongation of the plateau is a consequence of the presence of many short chains or dangling ends.

### *Visualization of defect structures*

The defect structure of the chains can directly be visualized by (negative staining) electron microscopy (Fig. 3 a)

and by fluorescence microscopy of fluorescently labelled actin (Fig. 3 b). Both microscopy techniques show that the F-actin filaments have a considerably number of sharp bends which are attributed to packing defects in the chains. These could be caused by insertion of additional monomers in one of the two strands.

Figure 3 ($a_1$ and $a_2$) shows negative staining micrographs of 150 μg/ml actin solution taken about 20 min after starting polymerization and after annealing for 2 h, respectively. The electron micrographs show clearly that the defect density is much higher (roughly 3 defects per 10 μm) for freshly polymerized actin than after annealing. Moreover, there is a clear difference between the lateral distribution of the filaments before and after annealing. The filaments are much less homogeneously distributed in the former case and appear to exhibit some microphase segregation.

There is always the danger of structural alterations during the rapid drying of the samples. This should affect the two solutions of different age in the same way. Thus, we can conclude that the degree of entanglement of a freshly prepared actin network is less extensive than in the annealed form.

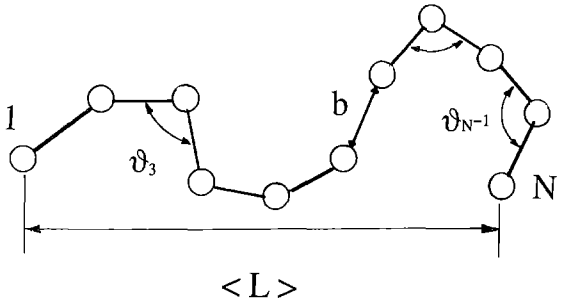


**Fig. 7.** Kramers "random walk" model of freely jointed bead-rod chains. $b_0$ is the Kuhn length. *Note:* The rods between joints can be assumed as semiflexible and exhibiting thermally driven bending undulations

*The evaluation of the polymerization process*

Time-dependent measurements of the viscoelastic parameters allow one to follow the actin polymerization in a quantitative way. This is first shown in Fig. 4 for pure actin on a log scale. The storage and loss moduli are measured continuously at a frequency of 0.7 Hz (e.g. within the regime determined by the internal chain dynamics). There is a remarkable difference in the behaviour of $G'$ (0.7 Hz) and $G''$ (0.7 Hz). While the former exhibits a long incubation period (from 0 to 400 s) with a $G'$ value characteristic for pure water, $G''$ already starts to increase 200 s after addition of F-buffer. This difference is more clearly revealed by the phase shift:

$$\varphi = \text{arc tg}\,\frac{G'}{G''}. \tag{4a}$$

The saturation point is reached at the same time ($t_{sat} = 8 \cdot 10^3$ s), both for $G'$ and $G''$. The difference between $G'(\omega)$ and $G''(\omega)$ is expected and yields useful information for the following reason: $G''$ is a measure of the intrinsic dynamic viscosity, $\eta(\omega)$ of the macromolecular solution according to:

$$\eta = G''/\omega. \tag{4b}$$

As is well-known, it is proportional to a power ($\varepsilon$) of the molecular weight of the polymer ($\eta \propto M^{\varepsilon}$) where $\varepsilon$ varies between 0.5 and 1 depending on the type of model (cf. Doi and Edwards 1986). In principle, the average length of the filament could be estimated as a function of time though for more quantitative analysis the length distribution would have to be known.

$G'(\omega)$ only exhibits a substantial value if the chains overlap, and the onset of the increase of $G'$ defines the time at which the average chain length becomes about equal to the mesh size, $\xi$. In Fig. 4, with $c_A = 300$ μg/ml, the mesh size $\xi$ equals 0.6 μm at $t = 5 \cdot 10^2$ s. The average chain length is ~1 μm. (Note: $G'(\omega)$ and $G''(\omega)$ were previously measured for both increasing and decreasing frequencies and showed no significant differences (cf. Müller et al. 1991).)

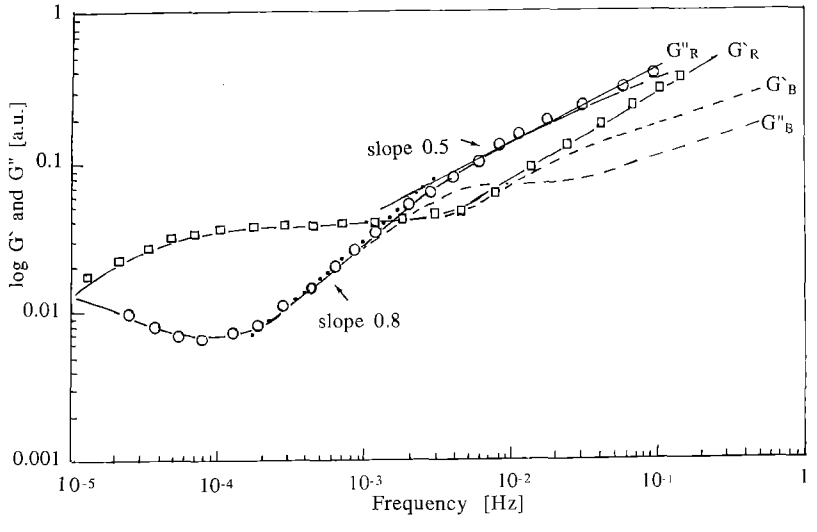


**Fig. 8.** Comparison of experimental and calculated frequency dependencies of storage modulus $G'(\omega)$ (*experimental data points* □–□) and loss modulus $G''(\omega)$ (*data points* ○–○) of entangled solutions of actin ($c_A = 300$ μg/ml). *Curves drawn* (——) are calculated by superimposing reptation and Rouse modes. *Dashed curves* (– – –) are calculated by superimposing reptation and bending modes. The best fit was obtained in both cases for a ratio of the terminal to the internal relaxation time of, $\tau_d/\tau_i \approx 2000$ and for the amplitude ratio of, $A \approx 10$. Since $\tau_d \approx 3 \cdot 10^4$ s, one obtains $\tau_i \approx 15$ s ($\omega_e \sim 0.07$ Hz).

*The effect of talin and vinculin on actin solutions*

Figures 5 and 6 show the modulation of the frequency-dependent viscoelastic moduli and the growth kinetics by talin and/or vinculin. In Fig. 5 a, b, the viscoelastic response $G'(\omega)$ and $G''(\omega)$ are for $c_A = 300$ µg/ml solution of pure actin polymerized in the presence of vinculin (at a molar ratio $r_{AV} = 7$), talin ($r_{AT} = 7$) and both vinculin and talin ($r_{AT} = r_{AV} = 10$).

For comparison variation of the storage modulus, $G'(\omega)$ caused by severing the actin chains is also shown for a solution of $c_A = 300$ µg/ml and $c_A = 700$ µg/ml. Note: These curves are shifted in the direction of the ordinate by one decade in each case. The most remarkable results of Fig. 5 a, b are:

- (A) Vinculin does not affect $G'(\omega)$ to a significant extent.
- (B) Talin (at $r_{AT} = 7$) has a strong effect at all frequencies. It does not suppress the plateau value of $G'(\omega)$ (as does severin) but causes only an elongation. However, the onset of the internal dynamics regime is shifted to higher frequencies by roughly two frequency decades as is most clearly revealed by the shift of the frequency regime $G''(\omega)$ and the slope of 0.8.
- (C) In contrast to talin, severin does not significantly affect the frequency position of the internal dynamics regime and therefore, $\tau_i$. It does, however, suppress the plateau regime completely.
- (D) The change of both $G'(\omega)$ and $G''(\omega)$ produced by talin is not modified noticeably when vinculin is also present.

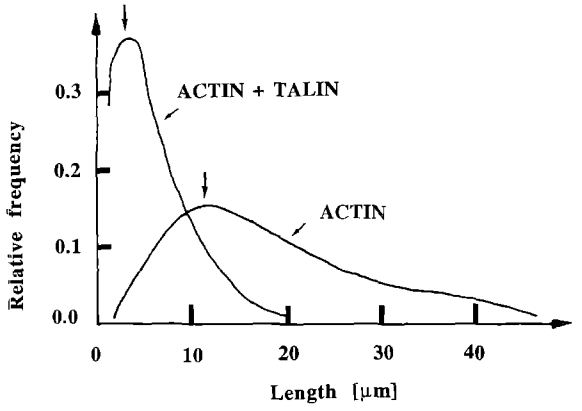


**Fig. 9.** Distribution of actin filament length of phalloidin labelled F-actin in the absence and presence of talin at actin:talin molar ratio $r_{AT} = 4$. Data were replotted from Kaufmann et al. (1992). The actin concentration was about $c_A = 200$ µg/ml. The contour length of the filaments was measured by image processing of fluorescence micrographs

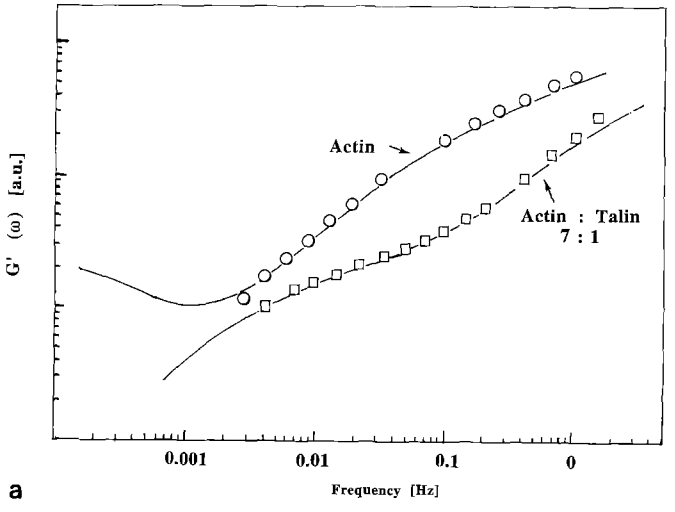


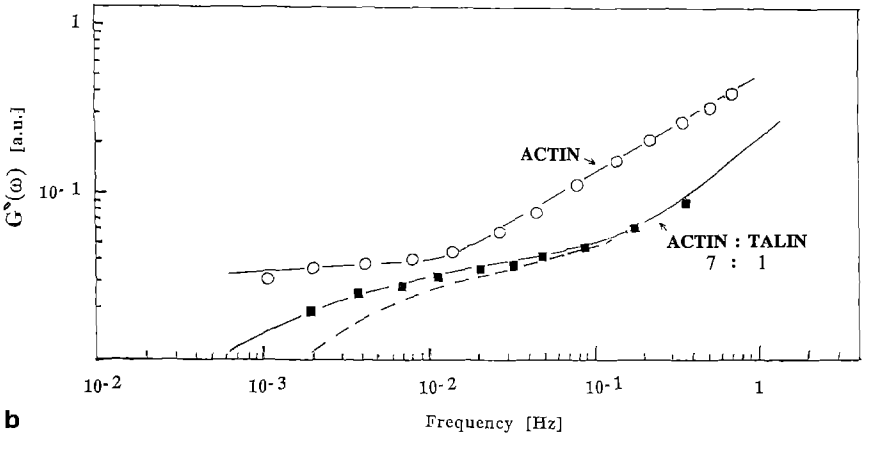


**Fig. 10 a, b.** Simulation of viscoelastic parameters of the system actin plus talin at an actin: talin molar ratio $r_{AT} = 7$ (data of Fig. 5 a) by superimposing the reptation and Rouse processes only. Figure 10 a presents the case of the storage modulus $G'(\omega)$ and Fig. 10 b for the loss modulus $G''(\omega)$. For comparison, the case of a second measurement of pure actin is also shown. The two adaption parameters, $\tau_d/\tau_i$ and, $A$ were the same for $G'(\omega)$ shown in **a** and for $G''(\omega)$ shown in **b** $\tau_d/\tau_i = 100$ and $A = 10$. *Note:* Frequency [Hz], $G'(\omega)$ and $G''(\omega)$ are on log scale

*Modification of growth kinetics*

Most remarkable is the effect of talin on the polymerization kinetics of actin shown in Fig. 6; an effect which has also been observed by Goldmann et al. (1992). In contrast to pure actin, $G'(\omega)$ and $G''(\omega)$ exhibit a finite value (about half the maximum value) immediately after starting polymerization. However, the subsequent increase of the viscoelastic moduli is much slower than for pure actin; in fact the increase lasts for many hours. Previous observations strongly suggest that short actin filaments are formed during the time ($\sim 5-10$ s) required to start the measurement (Kaufmann et al. 1991). The latter suggests that these short fragments eventually fuse to form long chains.

## Discussion

*Model of viscoelasticity of pure F-actin*

The measurement of both the viscoelastic moduli over five frequency decades and the three relaxation regimes – typical for semidilute high molecular weight polymer solutions – were more accurately determined than previously. It was verified that the frequency dependence of $G'(\omega)$ and $G''(\omega)$ in the regime determined by internal chain dynamics (at $\omega \geq 1/\tau_i \approx 0.5$ Hz) obeys the power law $G'(\omega) \sim G''(\omega) \propto \omega^{0.52 \pm 0.02}$ which is characteristic for Rouse-like chains. Previously various power laws were established relating: a) the relaxation times, $\tau_d$ and $\tau_i$ to the chain length, L; b) the height, $G_N^0$ of the rubber plateau to the monomer concentration (Müller et al. 1991) or c) the mesh size, $\xi$ to the monomer concentration (Schmidt et al. 1989). These data provided evidence that – if slow dynamic processes of time scales larger $\sim 1$ s are observed – F-actin solutions behave very similarly to entangled networks of highly flexible polymers (Graessley 1974). Further, the recent theory of bending excitations of semiflexible filaments by Farge and Maggs (1993) and previous dynamic light scattering studies of the internal chain dynamics of F-actin by Schmitt et al. (1989) provided very strong evidence that in the time domain of $10^{-5}\,\text{s} \leq t \leq 10^{-1}$ s, the chain dynamics are determined by bending excitations. Evidence for this interpretation was provided in a recent direct analysis of single filament excitations visualized by fluorescence microscopy. In a flicker spectroscopic study we found that – in the micrometer wavelength regime – the chain dynamics are determined by bending excitations. A bending stiffness of $B = 4.0 \cdot 10^{-27}$ J · m was reported, corresponding to a persistence length of $L_p = B/k_B T \approx 0.5$ μm (Schmidt et al. 1989). In the following paragraphs, we provide evidence that this apparent discrepancy between rheological studies and QELS can be understood in terms of a cross-over between semiflexible and highly flexible (Rouse-like) behaviour.

The finding of two relaxation processes separating a plateau ($\tau_d^{-1} < \omega < \tau_e^{-1}$) regime and an ascending branch of $G'$ and $G''$ can be best described in terms of a superimposed reptation process (Doi and Edwards 1986) and chain conformational excitations.

Consider first the reptation process based on a concept by de Gennes (1971): This model describes the motion of a single polymer filament in an entangled polymer solution as a snail-like migration of the single filament in a "tube" formed by the network of the other filaments. The motion is driven by the local excitations of the chain migrating. The tube is called the "primitive" tube and has the topology of the conformation of the chain considered.

The complex elastic constant is of the form (Doi and Edwards 1986):

$$G_R^*(\omega) = G_N^{(0)} \sum_{p,\,\text{odd}} \frac{8}{\pi^2} \frac{1}{p^2} \frac{\left(\frac{\omega \tau_d}{p^2}\right)^2 + i\left(\frac{\omega \tau_d}{p^2}\right)}{1 + (\omega \tau_d / p^2)} \tag{5}$$

where, $\tau_d$ is the terminal relaxation time and, $p$ is the number of the mode. In an entangled network with the end-to-end distance of the chain, $\langle L \rangle$ (being large compared to the mesh size), the amplitude, $G_N^{(0)}$ is given by the classical expression for the rubber elastic modulus:

$$G_N^{(0)} = \frac{c_A k_B T}{N_e} = \frac{\varrho R T}{M_e} \tag{6}$$

where, $N_e$ is the average number of monomers between two points of entanglement and, $M_e$ the corresponding molecular weight, $\varrho$ is the mass density of the polymer. This law has been verified for actin networks (Müller et al. 1991).

The terminal relaxation time is determined by the time required for the "primitive" tube to diffuse over a distance equal to its average length. Even for semiflexible filaments, the "primitive" tube is expected to exhibit characteristic features of a random Gaussian coil, for which Doi and Edwards (1986) derived the following expression:

$$\tau_d = \frac{6 \pi \eta_w (N b)^3}{\pi^2 k_B T} \left(\frac{b}{\xi}\right)^2 \propto \frac{N^3 b^5}{\xi^2} \tag{7}$$

Consider now the dynamics of chain conformations: The internal chain dynamics have to be described in terms of two contributions to the elastic potential, $F_{el}$ (Lagowski et al. 1991):

$$F_{el} = \frac{1}{2} B \int \left(\frac{\partial^2 \boldsymbol{R}(s)}{\partial s^2}\right)^2 ds + \frac{1}{2} K \int \left(\frac{\partial \boldsymbol{R}(s)}{\partial s}\right)^2 ds \tag{8}$$

where, $\boldsymbol{R}(s)$ denotes the position of the contour length in space. It is related to the local tangent, $\boldsymbol{t}(s)$, by $\boldsymbol{t}(s) = \partial \boldsymbol{R}(s)/\partial s$. The first term accounts for bending excitations and $B$ is the bending elastic modulus (units: J · m). The second term formally corresponds to an extensional deformation. It has been introduced in order to account for the quasi-random structure of the filaments. $K$, the elastic constant, is to be measured in units (J/m). The second contribution is completely analogous to the elastic potential of a Rouse chain of beads interconnected by (massless) entropy springs of average length, $b$. In this case, the elastic constant would be of the form $k = K/b = 3 k_B T/b^2$ (cf. Doi and Edwards 1986). For classical random coils the Rouse term would generally be dominant. However, for dynamic neutron scattering studies (QENS) the bending elasticity could well play a dominant role. This could

be one of the reasons why the $q$-dependence of the line width of the spin-echo spectrum (Richter et al. 1978) does not obey the $q^3$-law very well, but appears to exhibit a smaller exponent ($\sim 2.8$) as predicted for semiflexible coils by Schmidt et al. (1989) and by Farge and Maggs (1993).

The above energy expression introduces two length scales: The persistence length, $L_p$ and the segment length, $b$:

$$L_p = B/k_B T \quad \text{and} \quad b = \tfrac{1}{3} k_B T/K \tag{9}$$

Our basic assumption is now that on a large scale the actin filaments behave as Rouse-like chains. Firstly, random chain behaviour is expected owing to the rather high density of defects (average distance $\approx 5$ μm) leading to sharp bends of the chain. Judging from direct observation of fluorescently labelled actin filaments (Käs et al. 1993) the dihedral angle of the bend can fluctuate. Therefore, F-actin is expected to exhibit typical properties of the Kramers model of freely jointed, straight segments (cf. Fig. 7). Secondly, it has been shown by Lagowski et al. (1978) that the large scale excitations of worm-like chains can be described by the Rouse model, which is equivalent to the Kramers model.

In the Kramers model the flexibility is characterized in terms of the effective segment length:

$$b^2 = b_0^2 \frac{1+\langle\cos\vartheta\rangle}{1-\langle\cos\vartheta\rangle} \tag{10}$$

where, $b_0$ is the so called Kuhn length and, $\langle\cos\vartheta\rangle$ is the average angle between two adjacent bonds (cf. Fig. 7).

If one accepts that – on a large scale – the dynamics of F-actin can be approximated by the "random walk" model, the frequency dependence of the complex modulus can be calculated by the classical theory of solutions of flexible coils. This is very clearly demonstrated by Doi and Edwards (1986) and in more general form by Birds et al. (1987). The basic steps of this theory are summarized in the Appendix, where we calculate the frequency dependence of $G^*(\omega)$ for the case of the bending elasticity model. The calculation for the Rouse chain can be found in Doi and Edwards (1986).

For simplification we neglect the hydrodynamic interaction between the beads. This approximation is justified since we are only interested in the frequency dependence of $G^*(\omega)$. The difference in the exponent, $\alpha$ of the power law $G^*(\omega) \propto q^\alpha$ between situations with and without hydrodynamic interaction are smaller than the accuracy of our data.

The frequency dependence of the viscoelastic moduli $G'(\omega)$ and $G''(\omega)$ in the whole frequency regime is now determined by superimposing the reptation dynamics $G_R^*(\omega)$ and $G_i^*(\omega)$ according to:

$$G^*(\omega) = G_R^*(\omega) + G_i^*(\omega) \tag{11}$$

consideration of Eqs. (5) and (A.15) shows that the storage modulus is given, for instance, by:

$$G'(\omega) = G_N^{(0)} \sum_{p,\,\text{odd}} \frac{8}{\pi^2} \frac{1}{p^2} \frac{(\omega\tau_d/p^2)^2}{1+(\omega\tau_d/p^2)^2}$$

$$+ \frac{c_A}{N} k_B T \sum_p \frac{(\omega\tau_{i,p})^2}{1+(\omega\tau_{i,p})^2} \tag{12}$$

The loss modulus is obtained by taking the linear expressions in the nominator. The terminal relaxation time is given by Eq. (7) and the internal relaxation time, $\tau_i$ depends on the type of elastic contribution.

- For Rouse modes of the order of, $p$ (for definition of $p$ see Eq. (A. 5)) $\tau_{i,p}^B$, is (Doi and Edwards 1986):

$$\tau_{i,p}^R = \frac{6\eta_w N^2 b^2}{\pi K} \frac{1}{p^2} \tag{13}$$

  where $K = 3k_B T/b$ for ideal Rouse chains.
- For pure bending modes the relaxation time, $\tau_{i,p}^B$ has been derived in the Appendix:

$$\tau_{i,p}^B = \frac{6\eta_w N^4 b^4}{4\pi^3 B} \frac{1}{p^4}. \tag{14}$$

If both elastic contributions come into play one would have to replace, $\tau_{i,p}$ by:

$$\frac{1}{\tau_{i,p}} = \frac{1}{\tau_{i,p}^R} + \frac{1}{\tau_{i,p}^B}. \tag{15}$$

For short wavelength excitations, the Rouse modes prevail while long wavelength deformations are determined by the bending modes. One expects a cross-over between the two extreme cases at $\tau_{i,p}^R \approx \tau_{i,p}^B$, i.e. at a wavelength:

$$\Lambda_c = 2Nb/p_c = 2\pi\sqrt{B/K} = 2\pi\sqrt{L_p \cdot L_d}. \tag{16}$$

The right side is obtained since $L_p = B/k_B T$ and $K \approx k_B T/L_d$. If the mechanical relaxation was determined by the defects, $L_d$ would correspond to the average distance between defects. For very large wavelengths ($qL_p \ll 1$), where worm-like-chains behave as random coils, $L_d$ would be an effective segment length (Lagowski et al. 1991).

Based on flickering spectroscopy (Käs et al. 1993) and previous studies (Müller et al. 1991) the persistence length is of the order of $L_p \sim 0.3-1$ μm and the distance between the defects, $L_d \sim 5$ μm; $\Lambda_c$ therefore has the same order (μm). Since $\Lambda_c$ is clearly much larger than the reciprocal wavevector in QELS experiments ($q^{-1} < 0.1$ μm), the dynamic structure factor is expected to be determined by bending excitations.

The longest bending relaxation time at the cross-over wavelength of $\Lambda_c \sim 2\pi \cdot$ μm is of the order:

$$\tau_{l,c}^B = \frac{6\eta_w \Lambda_c^4}{16\pi^3 L_p} \sim 20\text{ s}.$$

This is appreciably smaller than the longest internal relaxation time of $\tau_i \sim 100$ s estimated from Fig. 1. It is, therefore, expected that the Rouse character becomes dominant in viscoelastic measurements. It would be essential to carry out the present type of rheological measurements at higher frequencies in order to evaluate the cross-over to the semiflexible regime.

In Fig. 8 the experimental curves $G'(\omega)$ and $G''(\omega)$ for $c_A = 300$ μg/ml are compared with calculated curves obtained by superimposing *a*) the reptation modes with

Rouse modes and *b*) the former with bending modes. It is clearly seen that in the frequency domain determined by the chain dynamics, the experimental curves can be much better fitted by the Rouse model than by the bending model. In particular the power law $G'(\omega)$ and $G''(\omega)$ $\propto \omega^{1/2}$ is fulfilled over a much larger frequency regime in the former case. For the bending model the slope at large $\omega$ is considerably smaller than that of the Rouse model, namely 0.35 instead of 0.5. For that reason it is not possible to fit the experimental data in the internal dynamic region by the bending model. The best fit is observed for a ratio of the fundamental relaxation times $\tau_d/\tau_i = 2000$ and of amplitudes of the Rouse mode to the reptation modes of $A = 10$.

*Modification by talin*

Consider the effect of talin on the viscoelastic modulus $G^*(\omega)$. As strongly suggested by previous QELS studies (Piekenbrock 1991; Kaufmann et al. 1991) and microfluorescence observations (Kaufmann et al. 1992) talin appears to exhibit two effects *a*) it reduces the average length and *b*) it produces filament stiffness. The former effect is shown in Fig. 9. It is observed that in the presence of talin the filaments exhibit a rather sharp, roughly exponential distribution of lengths, $P(L)$:

$$P(L) \propto e^{-L/\langle L_0 \rangle} \tag{17}$$

with $\langle L_0 \rangle \approx 5-10$ μm. In contrast, the length distribution of pure F-actin is very wide and exhibits a maximum at $\langle L_{max} \rangle \approx 12$ μm and an average length of about 20 μm.

Despite the reduction in average length by talin there is an important difference between the effect of talin and typical severing proteins (e.g. severin) on $G^*(\omega)$:

- Severin completely abolishes the rubber-like plateau at actin:severin ratios of $r_{AS} = 300$ at $c_A = 300$ μg/ml and of $r_{AS} = 200$ at $c_A = 700$ μg/ml (cf. Fig. 5 a). In contrast, the rubber plateau remains even at an actin-to-talin ratio of $r_{AT} = 7$. Only the terminal relaxation regime (where $G(\omega) \to 0$) is elongated.
- In the case of severin the terminal relaxation time, $\tau_d$ is shifted to shorter times whereas the internal relaxation time, $\tau_i$ does not change significantly as shown previously (Müller et al. 1991). In contrast, $\tau_i$ is drastically reduced by talin. This is most clearly demonstrated by the $G''(\omega)$-versus-$\omega$ plot in Fig. 5 b which shows that the regime with a slope of $dG''/d\omega \approx 0.8$ is shifted by about two decades to higher frequencies.

The shift in, $\tau_i$ and the elongation of the terminal relaxation regime by talin is clearly demonstrated by the simulation of $G'(\omega)$ and $G''(\omega)$ shown in Fig. 9. An optimal fit is again achieved by superimposing the reptation and Rouse modes and by assuming that the filaments exhibit an exponential length distribution. For the simulation, the length distribution shown in Fig. 9 was used.

Therefore, the contribution of the reptation process is simulated, for instance, by:

$$G_R^I(\omega) = \frac{G_N^0}{L_{max}} \sum_p \int_0^{L_{max}} \frac{8}{\pi^2} \frac{1}{p^2} \frac{(\omega \tau_d(L)/p^2)^2}{1+(\omega \tau_d(L)/p^2)^2} P(L)\, dL \tag{18}$$

with

$$\tau_d(L) = \tau_d^0 \cdot L^3/\langle L_0^3 \rangle. \tag{19}$$

In a similar way the Rouse and the bending excitation contributions were averaged over the length distribution.

An optimal fit of both $G'(\omega)$ and $G''(\omega)$ was obtained for the same amplitude ratio as for pure F-actin ($A = 10$) but for a strongly reduced ratio of the relaxation times; namely $\tau_d/\tau_i \approx 100$ instead of $\tau_d/\tau_i = 2000$.

What can we learn from the above analysis? According to Eqs. (7) and (13), the terminal ($\tau_d \propto N^3 b^5/\xi^2$) and the internal relaxation time ($\tau_{i,1}^R \propto N^2 b^3$) are both determined by the effective filament length $L = N \cdot b$ ($b$, effective segment length defined in Eq. (10)). Thus, the ratio of relaxation times is:

$$\frac{\tau_d}{\tau_{i,1}^R} \propto N \cdot \frac{b^2}{\xi^2}. \tag{20}$$

Since the mesh size, $\xi$ is essentially constant for $c_A = \text{const.}$, the origin of the change of the relaxation times (and their ratio) caused by talin could be *a*) a change in the number of segments, $N$, *b*) a change in the effective segment length, $b$ (defined in Eq. (10)) or *c*) a change in both parameters. Since the plateau regime is only stretched out by talin (in striking contrast to the effect of severin), the majority of the actin-talin filaments are long compared to the mesh size ($\xi \sim 1.2$ μm at $c_A = 300$ μg/ml) and, therefore, a change of $N$ is most probably not responsible for the large shift of $\tau_d/\tau_{i,1}^R$. Thus, we have to conclude that binding of talin to F-actin increases the effective segment length, $b$.

The onset of the internal dynamics regime (for instance of the regime with a slope of $d \log G''(\omega)/d\omega = 0.8$ in Fig. 8) is determined by the largest relaxation time, that is the relaxation time for the longest chains. For the following reason this also suggests that the effective length, $b$ is dramatically changed by talin. $\tau_d$ appears essentially constant, inspite of the decrease in $N$. This decrease must, therefore, be overcompensated by the increase of $b$. This also explains the strong increase of $\tau_{i,1}^R$ which changes with a higher power of $b$ than of $N$ ($\tau_{i,1} \propto N^2 b^3$). Since $\tau_d/\tau_i$ increases by a factor of 20, $b$ has to grow at least by a factor of five.

According to Eq. (10) and Fig. 7, the increase of the effective segment length can be explained as a consequence of the reduction of the flexibility of the filaments about the joints (determined by the defects) or as an increase of the distance between defects.

It should be noted that the shift of $\tau_{i,1}^B$ to longer times (by a factor of 10) could also be explained by an increase of the bending stiffness, both on the basis of the bending model and the Rouse model. Firstly, the bending model predicts that $\tau_{i,1}^B$ decreases with increasing bending modulus ($\tau_{i,1}^B \propto 1/B$). If $\tau_d$ is not affected by talin one would expect an increase of $B$ by a factor of 20. Secondly, the persistence length, $L_p$ is proportional to $B$ and an increase of $L_p$ would correspond to an increase in the effective segment length of the Rouse model (Lagowski et al. 1991). Evidence for an increase of the bending stiffness by talin was provided previously by QELS experiments (Kaufmann et al. 1991). A remarkable slowing down of the long

time decay of the dynamic structure factor was found and according to the theory by Farge and Maggs (1993), this corresponds to an increase in the bending modulus. Indeed, this increase of $B$ was recently verified directly by correlation spectroscopy of single filament fluctuations as will be shown in a forthcoming paper.

## Concluding remarks

One intention of the present work was to clarify why actin filaments behave a semiflexible rods if their dynamics are observed by QELS or flicker spectroscopy and as Rouse chains in rheological measurements in the long time limit. Another motivation was to clarify whether rheological measurements are suited to study effects of actin binding proteins on the stiffness of actin filaments and on the structure and dynamics of entangled actin networks.

We provide evidence that the viscoelasticity of the networks is determined by the defect structure which gives the filaments typical properties of random chains of the Kramers type (semi-freely jointed segments). It should be noted, however, that for large excitation wavelengths compared to the persistence length ($L_p$, i.e. of the order of the chain length, $L$) the mechanical relaxation would also be expected to obey the Rouse law since the chain behaves as a random coil at $qL_p \ll 1$. This is only a rather crude approximation since the distance between defects is a few micrometers and each filament consists only of at most ten segments. Certainly more rheological measurements, in particular at higher frequency, are required in order to probe the cross-over from the Rouse-like regime to the bending regime. The design of a new rheometer for this purpose is in process.

Talin shows major effects: *a*) on the steady state polymerization kinetics and on the transient binding kinetics of actin (Goldmann and Isenberg 1991; Goldmann et al. 1992), *b*) on the length distribution and the stiffness of actin filaments (Kaufmann et al. 1992) *c*) on charged lipid monolayers using the film balance technique (Dietrich et al. 1993); however, talin most likely does not bind all along actin filaments (unpublished EM observation):

- It promotes the rapid formation of short oligomers. Based on Fig. 6 oligomers of about 1 μm length are formed within approximately 1 min. These oligomers appear to form long filaments after approximately five hours. In contrast, the growth of pure actin filaments is completed after about two hours.
- The present as well as previous QELS studies suggest that the short chains co-exist for a long time with very long filaments.
- In the framework of our interpretation of the viscoelasticity in terms of Rouse-like behaviour, we find a remarkable increase in the stiffness of the chains (expressed in terms of the effective segment length). The stiffening is paralleled by a slight increase in the bending stiffness as suggested by QELS.

The nucleation and stabilization of actin filaments by talin has important consequences (cf. Isenberg and Goldmann 1992). The reduction in the chain dynamics could help to prevent the repulsion between the filaments due to undulation forces (Verde et al. 1992) and thus, favour the parallel arrangement of filaments.

## Appendix

*Relaxation spectrum of semiflexible rods*

As a most simple mechanical model of a semiflexible rod we consider a chain of beads interconnected by massless rods of bending stiffness, $B$ and length, $b$ (cf. Fig. 7).

In order to determine the relaxation spectrum we start from the well known expression for the shear stress, $\sigma_{ij}$ ($i$, index denoting plane of attack and $j$ direction of stress):

$$\sigma_{ij} = \frac{c}{N} \sum_{n=1}^{N} \left\langle \left( \frac{\partial U_{\text{Bend}}}{\partial \boldsymbol{R}_{ni}} \right)_i \boldsymbol{R}_{nj} \right\rangle \tag{A.1}$$

where, $c$ is the radius vector of the $n^{\text{th}}$ monomer. $\boldsymbol{R}_{ni}$ is the component of $\boldsymbol{R}_n$ in the direction, $i$. $U_{\text{Bend}}$ is the bending energy introduced in Eq. (8). The brackets $\langle \ldots \rangle$ denote the ensemble average over all configurations.

It is useful to introduce the radius vector, $\boldsymbol{R}(s)$ to characterize the position of segment, $n$. Since the local tangent to the filament is $\boldsymbol{t} = \boldsymbol{R}(s + \mathrm{d}s) - \boldsymbol{R}(s)$, one can write for the bending elastic energy:

$$G_{\text{Bend}} = \frac{1}{2} B \int_0^L \left( \frac{\partial^2 \boldsymbol{R}}{\partial s^2} \right)^2 \mathrm{d}s = \frac{1}{2} \frac{B}{b^3} \int_0^N \left( \frac{\partial^2 R}{\partial n^2} \right)^2 \mathrm{d}n \tag{A.2}$$

where the right side is obtained by inserting $\mathrm{d}s = b \cdot \mathrm{d}n$ (where $b$ is the segment length).

In the continuous limit one obtains from Eq. (A.1):

$$\sigma_{ij} = \frac{c}{N} \frac{1}{L} \int_0^L \left\langle \mathrm{d}s' \frac{\partial G_{\text{Bend}}(s')}{\partial s} |_i | \boldsymbol{R}(s')_j \right\rangle \tag{A.3}$$

where $\partial G / \partial s$ is the functional derivate of the left expression in Eq. (A.2) with respect to segment length, $s$. One, therefore, obtains finally:

$$\sigma_{ij} = \frac{cB}{NL} \int_0^L \left\langle \mathrm{d}s' \boldsymbol{R}_j(s') \int_0^L \mathrm{d}s \frac{\partial^4 \boldsymbol{R}(s)_i}{\partial s^4} \right\rangle. \tag{A.4}$$

Expansion of the deformation, $\boldsymbol{R}(s)$ in normal coordinates:

$$\boldsymbol{R}(s,t) = \boldsymbol{X}_0(t) + 2 \sum_{p=1}^{\infty} \boldsymbol{X}_p(t) \cos \frac{p \pi s}{L} \tag{A.5}$$

and insertion into Eq. (A.4) yields:

$$\sigma_{ij}(t) = \frac{c}{N} \sum_p 2 B_p \frac{\pi^4 p^4}{L^3} \langle \boldsymbol{X}_{pi}(t) \boldsymbol{X}_{pj}(t) \rangle$$

$$= \frac{c}{N} \sum_p b_p \langle \boldsymbol{X}_{pi}(t) \boldsymbol{X}_{pj}(t) \rangle \tag{A.6a}$$

with ($L = N \cdot b$):

$$b_p = \frac{2B\pi^4}{L^3} p^4. \tag{A.6b}$$

This equation is equivalent to the well known relationship for the Rouse model (Doi and Edwards 1986) with the exception that $b_p$ is replaced by $k_p = 3k_BT/L^2$.

The next problem is to calculate the mean square amplitude $\langle \boldsymbol{X}_{pi}(t)\boldsymbol{X}_{pj}(t)\rangle$. This is usually done by starting from the Langevin equation for each mode which reads:

$$\zeta_p \frac{\partial}{\partial t}\boldsymbol{X}_p(t) = -b_p \boldsymbol{X}_p(t) + \zeta_p \varkappa \boldsymbol{X}_p(t) + f_p(t) \tag{A.7}$$

where, $\zeta_p$ is the frictional constant of each segment of length $b$ and $\zeta_p = 6\pi\eta_w b$. $f_p(t)$ is the fluctuation force driving the flickering of the filaments. The second term on the right side accounts for the shear force due to the hydrodynamic flow excited by the external (oscillatory) excitation. $\varkappa$ is the tensor of the velocity gradient: $\varkappa_{ij} = \partial v_i(\boldsymbol{r}, t)/\partial x_j$ (Doi and Edwards 1986). In the present experiment, the amplitude of the external oscillatory force is small. If we denote by $z$ the rotational axis of the rheometer, by $x$ the local axis along the radial direction, and by $y$ the local angular direction (equal to the direction of the shear force), the velocity increases linearly in the $z$-direction and one has to consider only the tensor element $\varkappa_{xy}(r, t) = \dot{\alpha} r/h$ where $r$ is the radius of the local position considered (Müller et al. 1991) and $\dot{\alpha}$ is the shear rate.

In order to calculate the expression $\langle \boldsymbol{X}_{pi}(t)\boldsymbol{X}_{pj}(t)\rangle$ in Eq. (A. 6a) it is customary to consider the Smolukowsky equation. This procedure is very clearly described in Doi and Edwards (1986) for the Rouse model and will not be repeated here. It results in the following differential equation for $\langle X_{px}(t)X_{py}(t)\rangle$:

$$\frac{\partial}{\partial t}\langle X_{p,x}X_{p,y}\rangle = -2\frac{b_p}{\zeta_p}\langle X_{p,x}X_{p,y}\rangle + \varkappa_{xy}(t)\langle X_{p,y}^2\rangle. \tag{A.8}$$

This equation is further simplified by assuming that for small shear rates $\varkappa_{xy}(t)$, the ensemble average of the mean squared amplitude $\langle |X_{py}(t)|^2\rangle$ can be replaced by its thermodynamic equilibrium value. By insertion of Eq. (A. 5) in Eq. (A. 2), it is easily verified that the bending energy may be expressed in terms of the mean square amplitudes of the modes, $X_p$ as:

$$G = \frac{B}{2}\sum_p \left(\frac{2\pi^4 p^4}{N^3 b^3}\right)\langle X_p^2\rangle = \frac{1}{2}\sum_p b_p \langle X_p^2\rangle. \tag{A.9}$$

Application of the equipartition theorem yields, $\langle X_{py}^2\rangle = k_BT/b_p$ and the relaxation equation (A. 8) reads:

$$\frac{\partial}{\partial t}\langle X_{p,x}X_{p,y}\rangle = \frac{-1}{\tau_p}\langle X_{p,x}X_{p,y}\rangle + \varkappa_{xy}\frac{k_BT}{b_p} \tag{A.10}$$

where the relaxation time is:

$$\tau_p^B = \zeta_p/2b_p. \tag{A.11}$$

A general solution of Eq. (A. 10) is:

$$\langle X_{p,x}(t)X_{p,y}(t)\rangle = \frac{\varkappa_{xy}k_BT\tau_p}{b_p}(1 - e^{-t/\tau_p}). \tag{A.12}$$

By inserting (A. 12) in (A. 6) and considering that:

$$\sigma_{ij} = \int_0^t dt'\, G(t-t')\,\dot{\alpha}(t') \tag{A.13}$$

the relaxation function is obtained as:

$$G(t) = \frac{c}{N}\sum_p e^{-t/\tau_p^B}. \tag{A.14}$$

The Fourier components in, $\omega$ space are, thus:

$$G'(\omega) = \frac{c}{N}\sum_{p=1}^{\infty}\frac{(\omega\tau_p)^2}{1+(\omega\tau_p^B)^2}; \quad G''(\omega) = \frac{c}{N}\sum_{p=1}^{\infty}\frac{\omega\tau_p^B}{1+(\omega\tau_p^B)^2} \tag{A.15}$$

It is exactly the same equation as obtained for Rouse modes where the Rouse relaxation time is determined by, $\tau_p^R$ given in Eq. (A. 13).

If we consider a situation where both, the bending and the Rouse relaxation processes play a role, the equipartition theorem is:

$$\langle X_{p,x}X_{p,y}\rangle = \frac{k_BT}{b_p + k_p} \tag{A.16}$$

and the relaxation time in Eqs. (A. 14) and (A. 15) has to be replaced by:

$$\frac{1}{\tau_p} = \frac{1}{\tau_p^B} + \frac{1}{\tau_p^R}. \tag{A.17}$$

*Acknowledgements.* The present work was founded by the Deutsche Forschungsgemeinschaft (Is-25/7-1, SFB 266/C-5 and SFB 266/B2) and the Fonds of the Chemischen Industrie. We greatfully acknowledge helpful discussions with Drs. Helmut Strey and Josef Käs. We thank Dr. Stefan Kaufmann, Hulda Kirpal, Karin Scharpf and Helga Hirsch for the careful protein preparations. Special thanks go to Irene Sprenger for excellent electron micrographs. Severin was a gift of Prof. Michael Schleicher, University of Munich.

## References

Bird RB, Curtiss CF, Armstrong RC, Hassanger O (1987) Kinetic theory: Dynamics of polymer liquids. Vol 2, 2nd edn. Wiley, New York

Bradford M (1976) A rapid and sensitive method for the quantitation of μg quantities of protein utilizing the principle of protein-dye binding. Anal Biochem 72:248–254

Collier NC, Wang K (1982) Human platelet P235: A high Mτ protein which restricts the length of actin filaments. FEBS Lett 143:205–210

Dietrich C, Goldman WH, Sackmann E, Isenberg G (1993) Interaction of NBD-talin with lipid monolayers: A film balance study. FEBS Lett 324:37–40

Doi M, Edwards SF (1986) The theory of polymers dynamics. Oxford University Press, Oxford

Farge E, Maggs AC (1993) Dynamic scattering from semiflexible polymers. Macromolecules (in press)

Ferry JD (1980) Viscoelastic properties of polymers. 3rd edn. Wiley, New York

Gennes PG de (1971) Reptation of a polymer chain in the presence of fixed obstacles. J Chem Phys 55:572–579

Goldmann WH, Isenberg G (1991) Kinetic determination of talin-actin binding. Biochem Biophys Res Commun 178:718–723

Goldmann WH, Niggli V, Kaufmann S, Isenberg G (1992) Probing actin and liposome interaction of talin and talin-vinculin complexes: A kinetic, thermodynamic and lipid labeling study. Biochemistry 31:7665–7671

Graessley WW (1974) The entanglement concept in polymer rheology. Adv Polymer Sci 16:1–200

Isenberg G, Goldmann WH (1992) Actin-membrane coupling: a role for talin. J Muscle Res Cell Mot 13:587–589

Janmey PA, Hvidt S, Lamb J, Stossel TP (1990) Resemblance of actin-binding protein/actin gels to covalently crosslinked networks. Nature (Lond.) 345:89–92

Käs J, Strey H, Bärmann M, Sackmann E (1993) Direct measurement of the wave vector dependent bending stiffness of freely flickering actin filaments. Europhys Lett 21:865–870

Kaufmann S, Piekenbrock TH, Goldmann WH, Bärmann M, Isenberg G (1991) Talin binds to actin and promotes filament nucleation. FEBS Lett 284:187–191

Kaufmann S, Käs J, Goldmann WH, Sackmann E, Isenberg G (1992) Talin anchors and nucleates actin filaments at lipid membranes: A direct demonstration. FEBS Lett 314:203–205

Korn ED, Carlier MF, Pantolini D (1987) Actin polymerization and ATP-hydrolysis. Science 238:638–644

Lagowski JB, Noolandi J, Nickel B (1991) Stiff chain model – functional integral approach. J Chem Phys 95:1266–1269

MacLean-Fletcher SD, Pollard TD (1980) Identification of a factor in conventional muscle actin preparations which inhibits actin filament self-association. Biochem Biophys Res Commun 96:18–27

Müller O, Gaub HE, Bärmann M, Sackmann E (1991) Viscoelastic moduli of sterically and chemically cross-linked actin networks in the dilute to semidilute regime: Measurements by an oscillating disk rheometer. Macromolecules 24:3111–3120

Piekenbrock TH (1991) Untersuchung von Aktinnetzwerken und deren Wechselwirkungen mit aktinbindenden Proteinen mittels dynamischer Lichtstreuung und anderer optischer Methoden. PhD thesis. Technical University of Munich, Germany

Piekenbrock TH, Sackmann E (1992) Quasielastic light scattering study of thermal excitations of F-actin solutions and of growth kinetics of actin filaments. Biopolymers 32:1471–1489

Pollard TD, Cooper JA (1986) Actin and actinbinding proteins. A critical evaluation of mechanisms and function. Annu Rev Biochem 55:987–1035

Richter D, Hayter JB, Mezei F, Ewen B (1978) Dynamic scaling in polymer solutions investigated by the neutron spin-echo technique. Phys Rev Lett 41:1484–1487

Sato M, Schwarz WH, Pollard TD (1987) Dependence of the mechanical properties of actin/α-actinin gels on deformation rate. Nature (Lond) 325:828–830

Schmidt CF, Bärmann M, Isenberg G, Sackmann E (1989) Chain dynamics, mesh size and diffusive transport in networks of polymerized actin. A quasielastic light scattering and microfluorescence study. Macromolecules 22:3638–3648

Spudich JA, Watts S (1971) The regulation of rabbit skeletal muscle contraction. J Biol Chem 246:4866–4871

Verde F, Dogterom M, Stelzer E, Karsenti E, Leibler S (1992) Control of microtubule dynamics and length by cyclin A- and cyclin B-dependent kinases in xenopus egg extracts. J Cell Biol 118: 1097–1108

Wegner A (1982) Kinetic analysis of actin assembly suggests that tropomyosin inhibits spontaneous fragmentation of actin filaments. J Mol Biol 161:217–227